3 D Fokker-Planck Calculation of Combined Fast Wave/Lower Hybrid and Electron Cyclotron Current Drive in Tokamaks

R.W. HARVEY, S.C. CHIU, M.G. MCCOY,* G.D. KERBEL,*
G.R. SMITH,† and T.K. MAU‡
General Atomics
San Diego, California 92186-9784, U.S.A.

Abstract

In a non-reactor tokamak environment, lower hybrid current drive can be combined with electron cyclotron waves, both (1) to control the radial profile of LH current deposition, and (2) to enhance the current drive efficiency [Fidone *et al.*, Phys. Fluids **27** (1984) 2468]. A related rf synergy is the use of multiple LH spectra for radial profile control as demonstrated in the ASDEX tokamak [Söldner *et al.*, IAEA, Washington (1990) CN-53/E-1-1]. In a reactor environment, fast waves provide an appropriate primary current drive system which can penetrate radially to the plasma core, and can be combined with ECCD. We use the CQL3D Fokker-Planck code to study these processes. Modelings of LHCD radial profile control by "filling the spectral gap" with EC or with additional LH power are presented. In the reactor environment, a range of cases with combined fast wave and electron cyclotron waves are examined, but no useful synergisms are found.

1. Introduction

Synergism between two separately-injected lower hybrid spectra has been observed in the ASDEX tokamak, in that power injected at high $n_\parallel$ controls the radial location for deposition and current drive of low-$n_\parallel$ injected power [1]. In the JET tokamak, a synergistic increase of driven rf current was observed when ICRF heating power was injected into a discharge supported by lower hybrid driven current [2].

Theoretically, Fidone *et al.* [3] have proposed two general types of lower hybrid/electron cyclotron rf synergisms: (1) control of the radial deposition of lower hybrid power by production of a local electron tail with electron cyclotron power, thereby "filling the spectral gap" at that location, and (2) increasing the current drive efficiency beyond what can separately be achieved by these systems, by locating the ECCD resonant region in velocity-space at the high velocity edge of the LH plateau. In a reactor environment, LH power is heavily damped and may not penetrate to the plasma core [4]. It is then appropriate to consider the weakly damped FW for current drive, analogous FW/EC synergisms, and enhanced FW damping due to EC tail formation.

The synergistic processes can readily be explored with the CQL3D three-dimensional $(u_\parallel, u_\perp, \rho)$ Fokker-Planck code [5]. (Relative to the magnetic field direction $u_\parallel$, $u_\perp$ are parallel, perpendicular momentum-per-mass of electrons, and ρ is a radial variable.) This code incorporates ray tracing and QL diffusion for LH, FW, and EC waves.

Good agreement of the LH/LH synergistic process between theory and experiment has been previously reported [6], and is elaborated here. Radial current profile control of an LHCD supported discharge, by injecting EC power in an ASDEX/DIII–D-like environment,

*NERSC/Lawrence Livermore National Laboratory, Livermore, California.
†Lawrence Livermore National Laboratory, Livermore, California.
‡University of California, Los Angeles, California.

is demonstrated with the code. FW/EC synergisms are explored in reactor and in derated-reactor environments. No useful FW/EC synergisms are calculated in a full ITER-like environment. Analytic analyses are presented to support the computational results.

2. The CQL3D Code

The CQL3D/LH code consists of a 2D-in-momentum-space, relativistic, bounce-averaged, collisional/quasilinear Fokker-Planck equation solver run on a radial array of flux surfaces combined with LH/FW [7] and EC [8] ray tracing, thereby modeling the distortion of the electron distribution function f_e resulting from rf energy injected at the plasma periphery. Thus, account is taken of variations in f_e as a function of radius, poloidal angle, and two momentum-space directions. Radial transport effects have been included but are not reported here. CQL3D is similar to codes described in Refs. 9 and 10.

The steady state of f_e and the radial rf absorption profile are obtained by iteration between (1) the Guassian elimination solution of the Fokker-Planck equation for the steady state f_e at each flux surface

$$\frac{\partial f_e}{\partial t}\left(u_{\parallel 0}, u_{\perp 0}, \rho, t\right) = \left\langle \frac{eE_{DC}}{m} \cdot \frac{\partial f}{\partial \underline{u}} \right\rangle + \langle C(f)\rangle + \langle Q(f)\rangle = 0 \quad , \tag{1}$$

where $u_{\parallel 0}$, $u_{\perp 0}$ are momentum-per-mass of electrons at the outer equatorial plane of each flux surface, $\langle\ \rangle$ indicates a bounce-average; and (2) the rf energy transport equation integrated along a ray

$$\nabla \cdot v_g \mathcal{E} = -\int du\,(\gamma - 1)\,mc^2\,Q(f) \quad , \tag{2}$$

where v_g is the lower hybrid ray group velocity, $\mathcal{E}$ is the energy density. In Eq. (1), C is the full collision operator linearized about a Maxwellian distribution shifted in the $u_\parallel$-direction to conserve momentum in the electron-electron collision process. The temperature and density profiles of the "background" Maxwellian distributions are fixed. The quasilinear operator Q is the full operator for the finite gyroradius, Landau/transit-time-magnetic pumping (*i.e.*, zeroth cyclotron harmonic) interaction [11] generalized to include the effects of relativity. The launched spectrum of rf energy is discretized into a set of rays which are injected from the plasma periphery. The rays are further discretized into short length elements, each of which contributes to the operator Q, and the damping of the ray element is self-consistently obtained using Eq. (2). The damping rate agrees well with standard expressions. LH/FW rays are traced for multiple passes across the plasma as they mode convert to and from the other polarization and reflect at the plasma periphery, until the wave energy is absorbed. We consider circular plasma models in this report.

3. LH/LH Synergy in the ASDEX Experiment

In low density ($\bar{n}_e \sim 1.5 \times 10^{13}/\mathrm{cm}^3$) ASDEX discharges, complete replacement of the ohmically-driven current by LH-driven current is obtained using 750 kW of rf power injected from one of the two independent grill antennas with 90 deg phasing (giving main spectral lobe $n_\parallel \sim 2.20 \pm 0.35$, and a reverse lobe at $n_\parallel = -6.5 \pm 0.5$ containing 25% of the power) [1]. Using the experimentally-measured profiles of density and temperature, the main spectral lobe is calculated to be damped after several passes of the ray energy across the tokamak. Spectral gap filling results from the $n_\parallel$-shifting associated with the poloidal location of ray bouncing [12,13]. On account of the centrally peaked electron temperature, the LH deposition is necessarily localized near the magnetic axis.

By injecting additional power from a second grill at 180 deg phasing (giving $n_\parallel = 4.375 \pm 0.375$ and an equal reverse lobe), rf current deposition is radially broadened, as confirmed experimentally by reduction in internal inductance ℓ_i and by Li-beam measurement of the current profile [14]. CQL3D calculations elucidate the mechanism for this. Figure 1 shows the quasilinear diffusion coefficients from the combined 90 deg/180 deg phasing case. Figure 1 (a) indicates that rf momentum-space diffusion in the central plasma ($r \sim 0.1\,a$) is entirely due to the main lobe of the 90 deg radiation. Both the 90 deg counter lobe and the 180 deg power are absorbed before reaching $r = 0.1\ a$. Figure 1 (b) shows substantial 180 deg power remains at $r = 0.54\ a$. The resulting electron distribution of this minor radius is shown in the next figure (Fig. 2). It is seen that the 180 deg power is "filling the spectral gap," *i.e.*, raising the plateau in the region of the main 90 deg plateau.

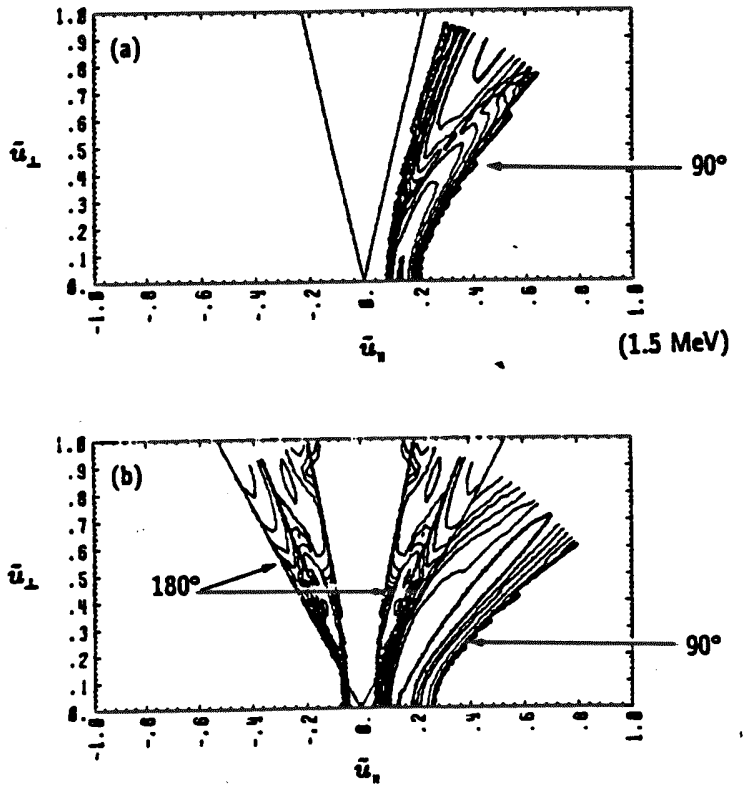

Fig. 1. Contour diagrams of QL diffusion coefficients evaluated (a) near the plasma center, and (b) at $r = 0.54\,a$, for combined injection of 90 deg and 180 deg LH spectra into an ASDEX discharge.

Figure 3 shows the power deposition and current drive resulting from the pure 90 deg and the 90 deg/180 deg cases. It is seen that the added 180 deg power actually reduced the central 90 deg power deposition and current drive by ~60%. This 90 deg power is deposited at $r \sim 0.5\,a$ driving current there, synergistic with the 180 deg heating power. Note also that some synergistic current is also driven at $r \sim 0.8\ a$. There, the combination of negative directed, high-$n_\parallel$, 90 deg counter lobe, with the 180 deg spectra and the 90 deg main lobe results in a positive current.

One may inquire as to a rough estimate of the power to "fill the spectral gap" at $r = 0.5\,a$, *i.e.*, in this case, the 180 deg power required to shift the 90 deg power absorption from the

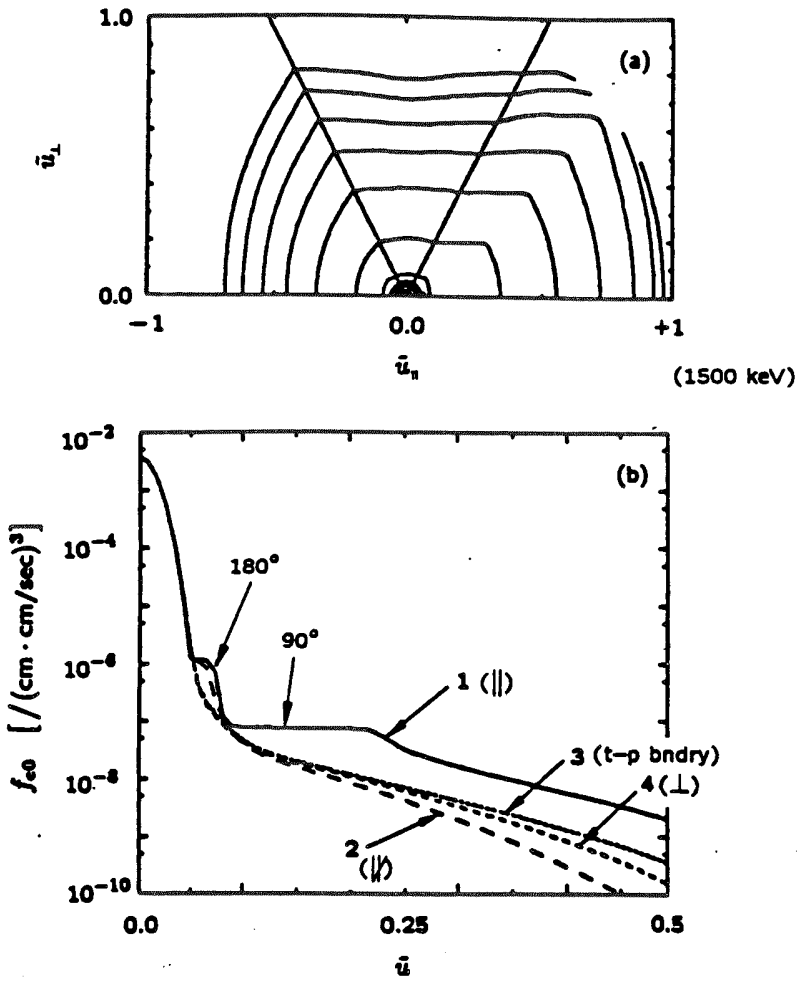

Fig. 2. (a) Contour diagram of f_e, and (b) cuts through f_e at constant pitch angle, 1 parallel to current direction, 2 anti-parallel, 3 at trapped-passing boundary, and 4 perpendicular.

plasma center to $r = 0.5\,a$. A 1D model for power P_{12} absorbed in producing a "plateau" in the range of parallel velocities (v_1, v_2), by parallel diffusion [15], gives

$$P_{12} = V \cdot \frac{n_e m_e v_{T_e}^2}{\tau_0}\, e^{-v_1^2/2v_{T_e}^2}\, \ell n\left(\frac{v_2}{v_1}\right) \quad ,$$

where V is the plasma volume in which the plateau is formed. Let P_{12} be less than the injected power with phase velocities in (v_1, v_2), and consider the situation in which additional rf power P_{01} with resonant phase velocities in (v_0, v_1) "fills the spectral gap" so that P_{12} is equal to the total of the power injected in (v_1, v_2). Then the ratio of the gap power P_{01} to the current drive power P_{12} is

$$\frac{P_{01}}{P_{12}} = \frac{\ell n(v_1/v_0)}{\ell n(v_2/v_1)} \quad .$$

Applying this equation to the present situation, we take $v_1 = c/\bar{n}_\parallel$, where $\bar{n}_\parallel$ is the average of the maximum $n_\parallel$ of the 90 deg main lobe and the minimum $n_\parallel$ of the 180 deg

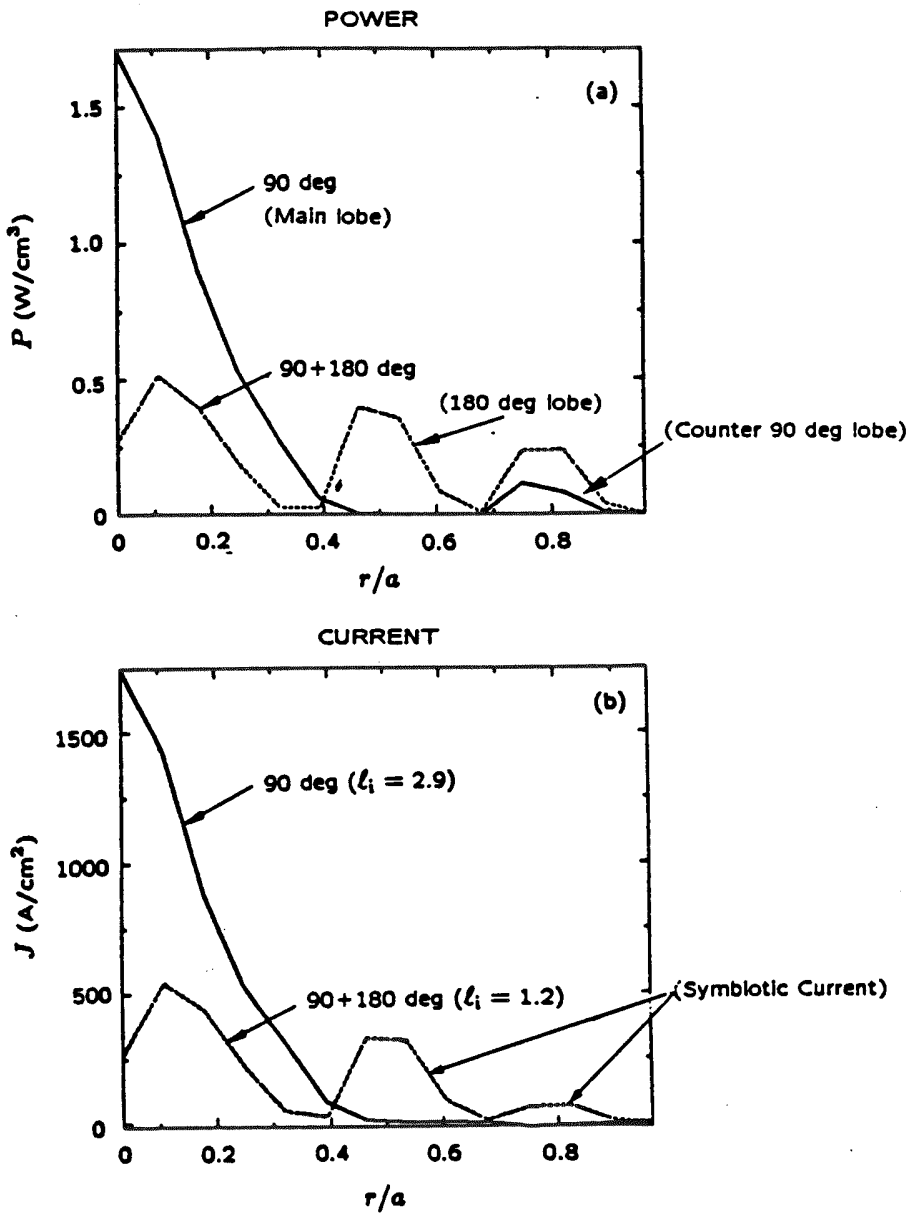

Fig. 3. Calculated LH (a) power deposition, and (b) current drive radial properties in the 90 deg and 90 + 180 degree phases.

spectral range. Thus, $P_{01}/P_{12} \approx \ell n(4.75/3.25)/\ell n(3.25/1.85) = 0.67$, in rough agreement with the code which itself is in good agreement with the experiment.

4. LH/EC Synergy

The velocity space region heated by EC radiation can be adjusted from far out in the electron tail down to zero velocity by varying $n_{\parallel}$ as given by the angle of injection. Figure 4 from Ref. 16 shows the range velocities satisfying the relativistic resonance condition

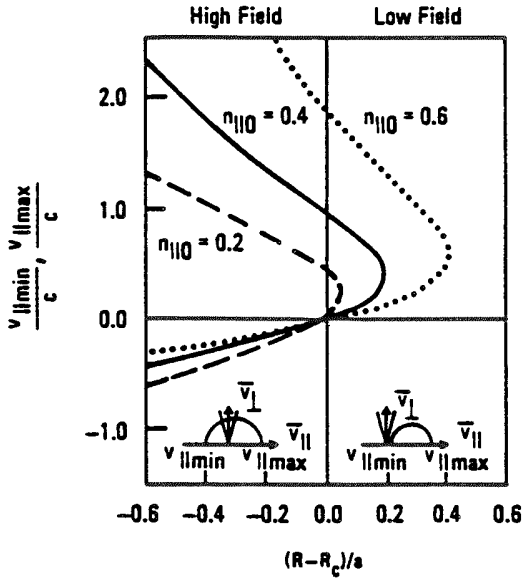

Fig. 4. The minimum and maximum $u_\|$ ($\equiv \bar{v}_\|$) on the resonance ellipse versus major radius distance from the cyclotron layer at R.

$\omega - k_\| v_\| - n\omega_{ce}/\gamma = 0$, where $v_\|$ is parallel velocity, γ is the relativistic factor. This equation is an ellipse in $u_\|, u_\perp$-space. This figure gives the minimum and maximum $u_\| \equiv \bar{v}_\|$ of this ellipse, for various $n_{\|0}$, the parallel refractive index evaluated at the resonance radius (major radius $R = R_c$, where $\omega = n\omega_{ce}$). The major radius variation of the magnetic field and $n_\|$ are both assumed to be proportional to R^{-1}. We refer to the major radius point (to the outboard side of R_c) at which $u_{\| min} = u_{\| max}$ as the *pinch point*. This point satisfies $(R_{pinch}/R_c)^2 = (1 - n_{\|0}^2)^{-1}$, and the electron energy at this point is given by the simple expressions $E_{pinch} = (\gamma_{pinch} - 1)mc^2$, $\gamma_{pinch} = (R_{pinch}/R_c)^2$.

For sufficiently high temperature (and density), radiation launched from the outboard side of the resonance layer in the fundamental O–mode or in the second harmonic X–mode, will be absorbed in the vicinity of the pinch point and/or before it reaches the $R = R_c$ layer. Thus, EC radiation is capable of heating tail electrons in a manner which is quite selective both in velocity- and in radial-space.

In this section we discuss a case of combined EC with LHCD, for control of the LH current drive radial profile. Evidently, unless LH radiation is single-pass absorbed, then it will be deposited predominantly near the plasma magnetic axis. We have modeled a situation to a DIII–D-like tokamak, of 0.5 MW LHCD with 2.0 MW of second harmonic X–mode EC. Plasma conditions are $\bar{n}_e = 1.4 \times 10^{13}\,cm^{-3}$, central electron temperature $T_{e0} = 2.2$ keV, $T_e(r = 0.6\,a) = 0.8$ keV. With solely the LH power, the driven current is 280 kA, localized to $r \lesssim 0.4\,a$.

The B-field and $n_\|$ have been adjusted so that the EC pinch point is at $0.8\,a$ and the cyclotron layer $R = R_c$ is at $r = 0.5\,a$. The pinch energy is at the low velocity end of the LH plateau. The EC current driven by 2 MW of the EC is only 10 kA, owing to the low temperature and toroidal trapping effects. This current peaks at $r = 0.75\,a$. The combined LH + EC current drive is 340 kA, showing a mild synergetic increase in total current (290 kA is the sum of the separate components), and with the dominant current now peaked at $r \sim 0.65\,a$. 140 kA is driven in the plasma core and 200 kA is now driven off axis due to the "filling of the

spectral gap" by the EC radiation. Only a few code runs of the above type have been carried out. The situation has not been optimized to minimize the necessary EC power required to obtain a given amount of off-axis LHCD.

5. FW/EC Synergy; ITER-like Scenarios

FW and EC powers injected separately and in combination with each other into an ITER-like plasma, have been simulated over a range of conditions, with the CQL3D code. For the FW, several cases of injection of power in different $n_\parallel$-ranges are considered. For the EC, combinations of outside launch, fundamental O–mode injections were considered in which the pinch point is at 100 or 400 keV, and the EC frequency is chosen so that the primary region of absorption is near the magnetic axis, or near $r \sim 0.5\,a$. In general, little synergy was obtained in the full reactor conditions: $R_0 = 6.5$ m, $a = 2.0$ m, $B_{T_0} = 5$ T, $n_{e0} = 1 \times 10^{14}\,\mathrm{cm}^{-3}$, $T_{e0} = 35$ keV, $Z_{\mathrm{eff}} = 1.5$, $P_{\mathrm{FW}} = 50$ MW, $P_{\mathrm{EC}} = 25$ MW. This result is discussed below. First, a scenario which is derated from full ITER-like parameters is considered in order to illustrate the physical conditions more clearly.

A case for which $n_{e0} = 5 \times 10^{13}\,\mathrm{cm}^{-3}$, $T_{e0} = 5$ keV is here examined. The deratings of both n_{e0} and T_{e0} increase the ratio of the fast wave to collisional velocity-space diffusion coefficient $D_{\mathrm{FW}}/D_{\mathrm{coll}}$, thereby increasing the quasilinear (QL) enhancement of the electron distribution beyond a Maxwellian and facilitating synergistic effects. Thus, as will be discussed further below

$$\frac{D_{\mathrm{FW}}}{D_{\mathrm{coll}}} \propto \frac{v_\parallel\, v_\perp^4}{n_e^{3/2}\, T_e} \frac{P_{\mathrm{FW}}}{(\omega/\omega_{\mathrm{ci}})} \quad , \tag{3}$$

where P_{FW} is the injected FW power and $(\omega/\omega_{\mathrm{ci}})$ is the ratio of wave frequency to ion cyclotron frequency. QL enhancement of the electron tail by EC radiation is also favored at low density. A stringent criterion

$$P_{\mathrm{EC}}\ (W/\mathrm{cm}^3) \gtrsim 0.5\ \left[n_e\ (10^{13}\ \mathrm{cm}^{-3})\right]^2 \quad , \tag{4}$$

for QL enhancement of EC current drive efficiency has previously been obtained [16], assuming that the minimum parallel velocity $v_{\parallel\,\mathrm{min}}$ on the resonance ellipse is $\sim 2\,v_{T_e}$. Since $D_{\mathrm{EC}}/D_{\mathrm{coll}} \propto P_{\mathrm{EC}} u_\perp^2 u_\parallel^2/n_e T$, the above power threshold for quasilinear effect decreases at constant $n_e \propto 1/v_{\parallel\,\mathrm{min}}^2$.

Figure 5 shows contour plots of the quasilinear diffusion coefficients and cuts through the 2 D electron distribution function at constant pitch angle, for the cases of (a) FW alone and (b) EC alone, at a flux surface at $r = 0.1\,a$. This is a case in which FW absorption is significantly increased by the application of EC power. Thus with solely the FW injected in $n_\parallel = 1.1$ to 1.25, there is very little absorption — 0.08% after $\approx$ 30 passes of the radiation across the tokamak. Choosing EC radiation with pinch point at $R_{\mathrm{pinch}} - R_0 = 30$ cm, $E_{\mathrm{pinch}} = 100$ keV, the EC quasilinear diffusion coefficient extends from $\tilde{u}_\parallel = 0.04$ to 0.35 ($\tilde{u}_\parallel \equiv u/u_{\mathrm{norm}}$, $u_{\mathrm{norm}} = 3.8\,c$, the momentum-per-mass which corresponds to 1.5 MeV). Plots in Fig. 5 are for $r = 25$ cm. EC power density at this location is 1.0 W/cm^3. Distortion of f_e from Maxwellian occurs beyond $\tilde{u} \approx 0.12$ ($v_\parallel \approx 4\,v_{T_e}$). 60% of the EC power is absorbed below $\tilde{u}_\parallel = 0.12$ where it causes no non-Maxwellian distortion (this situation may be unavoidable). Figure 6 shows f_e resulting from the combined FW + EC, both as a $u_\parallel, u_\perp$-space contour diagram, and again as cuts through f_e at constant pitch angle. The electron tail due to the FW power has been increased by 3 to 4 orders of magnitude. FW power absorption has been increased from 0.08% to 20%. Thus, this demonstrates a substantial synergistic increase in FW absorption. Fine

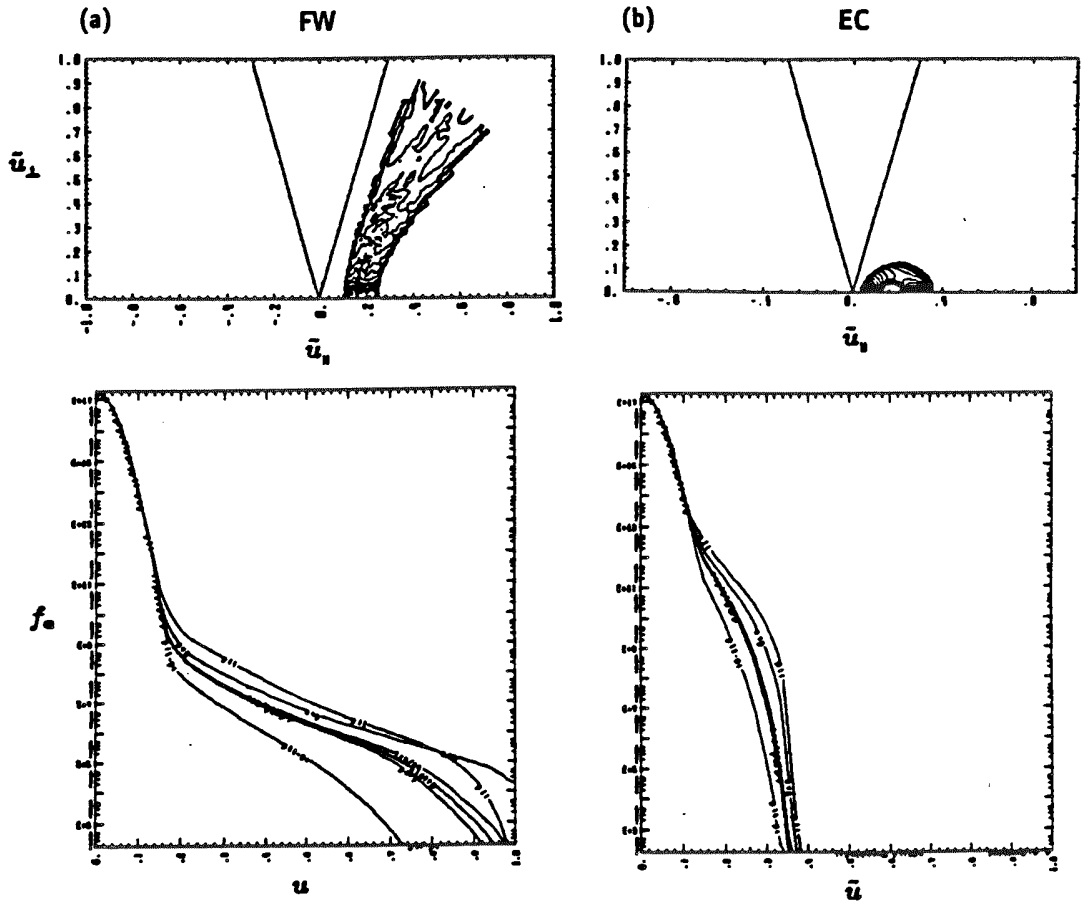

Fig. 5. Contour diagrams of QL diffusion coefficients and the resulting non-Maxwellian electron distribution plots for the cases of (a) solely FW, and (b) solely EC. For f_e, curves labeled "pll" refer to parallel pitch angle, "pll-pi" to anti-parallel pitch angle, "avg" is pitch angle average. $\bar{u}_\parallel$ corresponds to energy 1.5 MeV.

tuning of EC wave parameters may increase the FW absorption, however the present current drive is very peaked on axis, all the current being driven at $r \lesssim 0.2\,a$.

Under the same plasma conditions, if $n_\parallel$ of the EC radiation is increased so that the pinch is at 400 keV, then there arises the difficulty of inadequate absorption of the EC, even in the presence of the FW-induced tail. Table I gives a synopsis of CQL3D FW/EC results. The above lower density and temperature cases are summarized in the final box of the table.

As reported in the table, two additional plasma conditions were examined: (1) n_{e0} = 1. x 10^{14} cm^{-3}, T_{e0} = 35 keV, and (2) n_{e0} = 5. x 10^{13} cm^{-3}, T_{e0} = 35 keV. Both the FW and the EC radiation were entirely absorbed in all these cases. The FW and on-axis EC cases separately gave quite high efficiency: code run it 27 gives η_0 to 0.65 x 10^{20} (A/m^2·W) for FW, and code run it 02 η_0 to 0.54 x 10^{20} (A/m^2·W) for EC. Note that η_0 is defined using the central electron density; for the more usual case entailing line average density, multiply these results by ≈ 0.8.

However, no significant FW/EC synergies were found in any of these cases. That is, the resulting current drive in all these combinations was simply the sum of the separate FW and EC cases.

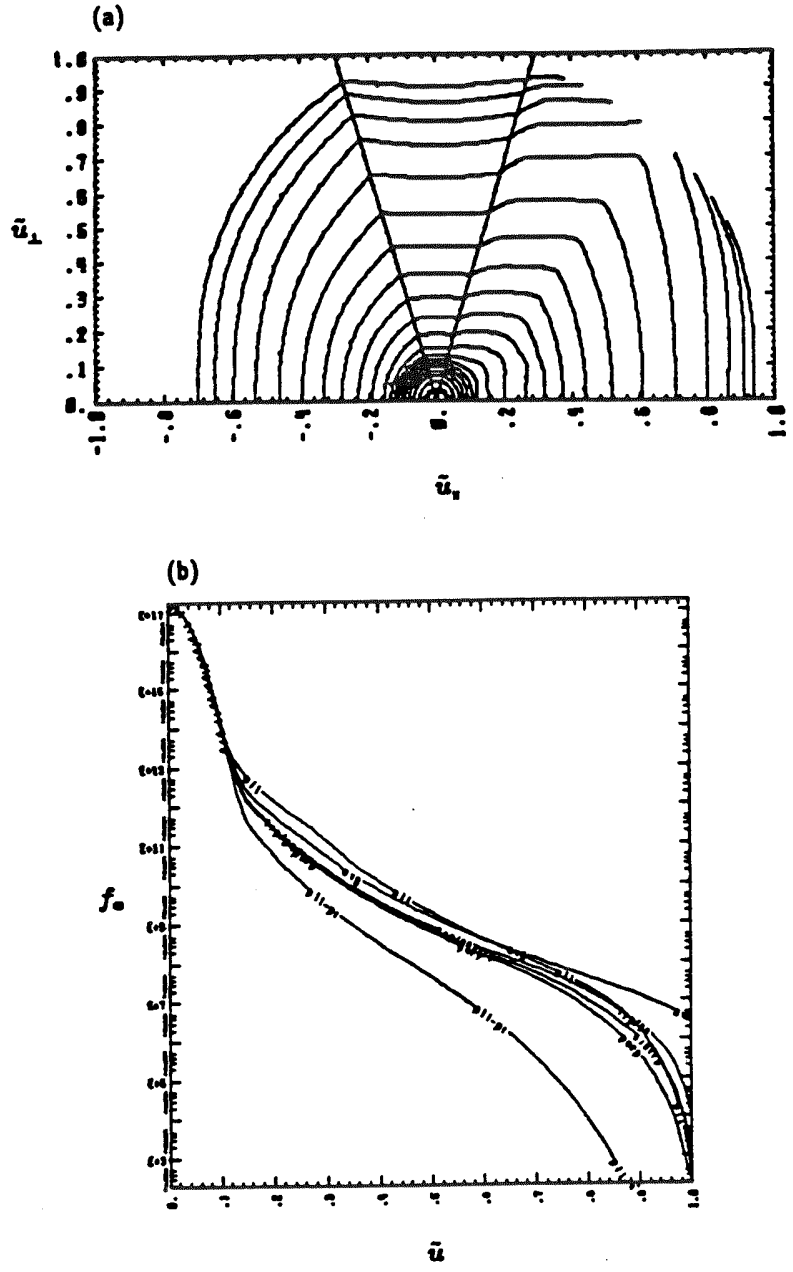

Fig. 6. (a) Contour diagram of f_e, and (b) cuts through f_e, corresponding to combining the FW and EC radiation of Fig. 4. f_e plots are labeled as in Fig. 5.

The code results summarized in Table I in the third horizontal box (code runs designated it06 through it28) illustrate the situation. The FW run it06 and EC run it02 both had complete, centrally localized, single pass absorption. At $\tilde{u}_\perp = 0$, the FW diffusion coefficient extended from $\tilde{u}_\parallel = 0.08$ to 0.2 near the plasma center, whereas the electron distribution was distorted from its Maxwellian value only at $\tilde{u} > 0.5$ (here $E_{\rm norm} = 1500$ keV, which gives $u_{\rm norm} = 3.8$ c, and $v_{T_e}/u_{\rm norm} = 0.07$). That is, $D_{\rm FW}$ only exceeds $D_{\rm coll}$ at high u, consistent with Eq. (3). $D_{\rm EC}$ extends from $\tilde{u}_\parallel = 0.2$ to 0.7, and thus might be hoped to result in

Table I: FW/EC Current Drive CQL3D Cases

(Applied power 50 MW at 58 MHz and/or 25 MW EC; $R_0 = 6.5$ m, $a = 2.0$ m, $B_{T_e} = 5$ T, $Z_{\rm eff} = 1.5$)

Description	Run	n_{e0} (10^{14}/cc)	T_{e0} (keV)	Abs. Pwr (MW)	Current (MA)	η_0	Comment
FW ($n_\parallel$: 1.2–3.2)	it 05	1.0	35.	50.	2.7	0.35	$\eta_0 = n_{e0} IR/P$
FW ($n_\parallel$: 1.1–1.5)	it 27	1.0	35.	50.	5.0	0.65	High rf efficiency
FW ($n_\parallel$: 1.2–1.5)	it 06	1.0	35.	50.	4.3	0.56	High rf efficiency
EC (0.0 a, 400 keV)	it 02	1.0	35.	23.7	1.95	0.54	High rf efficiency
FW + EC	it 07	1.0	35.	74.	6.20	0.54	Linear FW + ECCD (no synergy)
EC (0.5 a, 100 keV)	it 03	1.0	35.	35.	0.70	0.13	
FW + EC	it 28	1.0	35.	84.	5.00	0.39	(no synergy)
FW ($n_\parallel$: 1.2–1.5)	it 09	0.5	35.	50.	8.7	0.56	
EC (0.0 a, 400 keV)	it 10	0.5	35.	24.2	3.5	0.46	
FW + EC	it 11	0.5	35.	74.1	12.0	0.53	Linear FW + ECCD (no synergy)
EC (0.5 a, 100 keV)	it 14	0.5	35.	28.	1.10	0.13	
FW + EC	it 15	0.5	35.	78.	9.41	0.39	Linear FW + ECCD (no synergy)
FW ($n_\parallel$: 1.2–1.5)	it 16	0.5	5.	0.43 (30 bounces)	0.030	0.023	Central $n_\parallel$: 1.65–3.10
FW ($n_\parallel$: 1.1–1.25)	it 20	0.5	5.	0.039	0.035	0.29	Central $n_\parallel$: 1.65–2.5
EC (0.0 a, 100 keV)	it 25	0.5	5.	26.8	0.88	0.107	
FW + EC	it 26	0.5	5.	34.0	1.56	0.150	25 MW EC + 9 MW FW (synergetic increase in FW absorption)
EC (0.0 a, 400 keV)	it 23	0.5	5.	7.83	0.094	0.039	Shinethrough. Absorption peaked at $-0.8\,a$
FW + EC	it 24	0.5	5.	8.94	0.122	0.044	FW absorption increases from 39 to 442 kW.

synergistic current drive, à la Fidone *et al.* [3]. However, due to the small QL effects of the FW, no additional current arises in the combined FW + EC run (it 07).

The other synergy which has been envisioned [3] is radial profile control of the FWCD. An attempt at this is given by the additional runs it 03 and it 28, in Table I. The EC absorption is well-localized near $r = 0.5\,a$. But owing to the relatively large volume of the flux surfaces situated toward the plasma periphery, for a given flux surface thickness Δr, the dilution of the EC power gives power density $P_{EC} \leqslant 0.5$ W/cm^3. The density at $r/a = 0.5$ is $n_e = 0.88 \times 10^{14}$/cm^3. Consistent with the criterion in Eq. (4), there is no perceptible modification of f_e from its Maxwellian value. Hence, there is no change in the radial deposition and current profiles of the FW, *i.e.*, no synergetic profile control.

The same general results are obtained at $n_{e0} = 5 \times 10^{13}$ cm^{-3} and $T_{e0} = 35$ keV, as at the higher density.

The lack of synergism in a reactor environment can be understood from the following analyses. In order for the EC enhancement of FWCD efficiency by placing EC resonance at the high velocity end of the velocity region of FW diffusion to be useful, there must at least be a FW plateau formed. It is not credible that the FW is going to bounce back and forth in the tokamak cross-section more than 10 or 20 times without substantial, secular $n_\parallel$-variation due to density fluctuations and/or non-axisymmetries. The wave plane velocity would be reduced to values where there is significant absorption. For example, the condition for 10% single pass absorption under the reactor conditions considered here ($n_e = 10^{14}$ cm^{-3}, $T_e = 35$ keV, $B = 5$ T) is $2\,Im(k_\perp) \cdot a/2 = 0.1$, where $Im(k_\perp)$ gives the spatial damping rate. Thus,

$$2\pi^{1/2}\, k_\perp \beta_e\, \xi_e\, e^{-\xi_e^2}\, a = 0.1$$

where $\xi_e \equiv v_\parallel/(2^{1/2}\, v_{T_e})$, which gives $\xi_e = 2.5$. Using this value of $v_\parallel$ in the expression for the ratio of diffusion coefficients gives:

$$\frac{D_{FW}}{D_{coll}} = \frac{(\pi e^2/2\,m_e^2)\,(k_\parallel u_\perp/\omega\gamma)^2}{(3/2)\,(v_{T_e}^2/\tau_D)} \left| iE_y J_1\left(\frac{k_\perp u_\perp}{\omega_{ce}}\right)\right|^2 \frac{\gamma}{|u_\parallel|}\,\gamma\,(k_\parallel - k_{\parallel\,res}) \quad ,$$

$$\simeq \frac{(\pi e^2/2\,m_e^2)\,(k_\parallel u_\perp/\omega\gamma)^2\ (1/4)\ (k_\perp^2 u_\perp^2/\omega_{ce}^2)\ |E_y|^2/[\omega(\Delta k_\parallel/k_\parallel)]}{(3/2)\ (v_{T_e}^2/\tau_D)} \quad ,$$

$$= \frac{1}{35} \quad ,$$

assuming a single pass of 50 MW of FW power, and $\Delta k_\parallel/k_\parallel = 0.2$. This low ratio shows that no significant QL effects are expected.

Alternatively, considering synergistic FWCD radial profile control by application of EC at the low phase velocity end of the FW spectra, then as we have seen above, and from Eq. (4), prohibitive amounts of EC power are required.

6. Conclusions

Synergistic, radial profile control of driven LH current by injection of a second low phase velocity spectrum of power was demonstrated in the ASDEX. This process has been modeled in detail, and with essentially no free parameters, by the CQL3D Fokker-Planck code. The success of the modeling effort demonstrates the utility of this type of code for interpretation and prediction of rf experiments.

Synergistic LH current profile control by EC was illustrated by CQL3D in a DIII–D-like environment. A substantial, synergetic increase in FW absorption by central deposition of

EC power in an $n_{e0} = 5 \times 10^{13}\,\mathrm{cm}^{-3}$, $T_{e0} = 5$ keV, ITER-size plasma, was illustrated with CQL3D. 25 MW of EC power was employed. The required power for this synergism scales as R_0^{-1}, and hence 1/4 of this power would be required for a DIII–D-like tokamak ($R_0 = 1.7$ m). No useful FW/EC synergisms were obtained in a reactor- (ITER-) like environment. Good efficiencies ($\eta_0 \sim 0.5$ to 0.6) were obtained for both EC and FW in a reactor-like environment.

7. Acknowledgments

R.W.H. gratefully acknowledges helpful conversations, and computer sessions, with Dr. Marco Brambilla in adapting his LH/FW ray tracing code for use with the CQL3D Fokker-Planck code.

This is a report of work sponsored by the U.S. Department of Energy under Contract Nos. DE-AC03-89ER51114 and W-7405-ENG-48, and Grant No. DE-FG03-86ER-52126.

8. References

[1] F.X. Söldner *et al.*, Proc. 17th EPS Conf. on Controlled Fusion and Plasma Heating (Amsterdam, 1990), Vol. 14B, pt. 3, p. 1223.
[2] C. Gormezano *et al.*, *Radio-Frequency Power in Plasmas* (Proc. 9th Top. Conf., Charleston, 1991).
[3] I. Fidone *et al.*, Phys. Fluids **27** (1984) 2468.
[4] R.W. Harvey *et al.*, Proc. 3rd Top. Conf. on RF Plasm Heating (Pasadena, 1978), paper A7.
[5] G.D. Kerbel and M.G. McCoy, Phys. Fluids **28** (1985) 3629; M.G. McCoy *et al.*, AIP Conf. Proc. **159** (1987) 77; R.W. Harvey *et al.*, *ibid.*, 49.
[6] F.X. Söldner *et al.*, Proc. 13th Int. Conf. on Plasma Physics and Controlled Thermonuclear Fusion Washington, 1990 (IAEA, Vienna, 1991) Vol. I, p. 613.
[7] M. Brambilla, Comput. Phys. Rep. **4** (1986) 71.
[8] R.C. Meyer *et al.*, Nucl. Fusion **29** (1989) 2155 (see Appendix).
[9] M.R. O'Brien, M. Cox, and J.S. McKenzie, Nucl. Fusion **31** (1991) 583.
[10] G. Giruzzi, A. Bercoulet, D. Moreau, and B. Saoutic, Proc. of IAEA TCM on Reactor Scale Tokamaks, Arles, 1991 (IAEA, Vienna, 1992).
[11] C.F. Kennel and F. Engelmann, Phys. Fluids **9** (1966) 2377; I. Lerche, Phys. Fluids **11** (1968) 1720.
[12] P.T. Bonoli and R.C. Englade, Phys. Fluids **29** (1986) 2937.
[13] E. Barbato and F. Romanelli, Phys. Fluids B **2** (1990) 2687.
[14] Kent McCormick, personal communication (1989).
[15] N.J. Fisch, Rev. Mod. Phys. **59** (1987) 175.
[16] R.W. Harvey *et al.*, Phys. Rev. Lett. **62** (1989) 426.

Proceedings
of the

IAEA Technical Committee Meeting on

Fast Wave Current Drive in Reactor Scale Tokamaks

(Synergy and Complementarity with LHCD and ECRH)

ARLES (FRANCE) September 23 - 25, 1991

Edited by D. Moreau, A. Bécoulet, Y. Peysson

Association EURATOM-CEA sur la Fusion - Centre d'Etudes de Cadarache
13108 St Paul lez Durance CEDEX - FRANCE

Proceedings réalisés avec le soutien

du Ministère de la Recherche et de la Technologie
Délégation à l'Information Scientifique et Technique

1 rue Descartes, Paris (France)